ARTICLE

Solvatomorphism, polymorphism and spin crossover in bis[hydrotris(1,2,3-triazol-1-yl)borate]iron(II)

Received 00th January 20xx,
Accepted 00th January 20xx

DOI: 10.1039/x0xx00000x

Oleksandr Ye. Horniichuk, [ab] Karl Ridier, [b] Gábor Molnár, [b] Volodymyr O. Kotsyubynsky, [d] Sergiu Shova, [c] Vladimir M. Amirkhanov, [a] Il'ya A. Gural'skiy,*[a] Lionel Salmon, *[b] Azzedine Bousseksou [b]

Solvatomorphism and polymorphism play a crutial role in defining charachteristics of spin crossover (SCO) in coordination compounds. In this paper we describe a detailed characterization of the SCO bis[hydrotris(1,2,3-triazol-1-yl)borate]iron(II) complex ([Fe(HB(1,2,3-tz)$_3$)$_2$]) **1**. Five solvatomorphs of **1·2Solv** (where Solv = DMSO, MeOH, $CHCl_3$), **1·7DMSO** and **1·2DMF·H$_2$O** were obtained *via* recrystallization from the respective organic solvents. Solvatomorphs **1·2MeOH** and **1·2CHCl$_3$** undergo single-crystal-to-single-crystal transformations leading to **1** upon heating above 313 K. Single-crystal X-Ray diffraction analysis revealed π-π stacking and C–H···N contacts between molecules of the complex both in the solvated and desolvated crystals. Spin crossover and thermal properties of **1** and its solvates were investigated by means of calorimetry, thermogravimetry, Mössbauer spectroscopy, variable temperature magnetic susceptibility, Raman spectroscopy and powder X-Ray diffraction measurements. The anhydrous [Fe(HB(1,2,3-tz)$_3$)$_2$] complex, obtained via dehydration of the dodecahydrate, undergoes structural phase transitions upon the first heating in the 303-493 K range followed by reversible, gradual spin crossover upon further thermal cycling, with a transition temperature of $T_{1/2}$ = 373 K.

Introduction

Switchable molecular materials showing spin crossover (SCO) properties[1] attract attention of many research groups as they can be used for fabrication of functional devices, finding their application in information storage, molecular electronics, photonics, sensing and construction of mechanical actuators.[2–6] In this context, the ability to fabricate high quality, pure and homogeneous thin films of SCO materials is crucial. To this aim, vacuum thermal deposition provides a powerful means.[7,8] However, there are only a handful of spin crossover complexes that could be deposited by this technique.[9-23] Among these, only a few sublimable SCO complexes undergo spin transition above room temperature, namely [Fe(pypyr(CF$_3$)$_2$)$_2$(phen)] (pypyr = 2-(2'-pyridyl)pyrrolide, phen = 1,10-phenanthroline),[15] [Fe(HB(pz)$_3$)$_2$] (pz = pyrazolyl-1-yl)[22,23] and [Fe(HB(1,2,4-tz)$_3$)$_2$] (tz = triazol-1-yl),[21] the two latter belonging to the tris(1-azolyl)borate family of compounds.[24] For Fe-pypyr thin films, the transition temperature $T_{1/2}$ is reduced from 390 K for the bulk compound to approximately 330 K, whereas the two other complexes display similar SCO properties in bulk and thin film forms ($T_{1/2}$ ≈ 393 K and 335 K for the pyrazolyl and triazolyl derivatives, respectively). Notably, the high-quality thin films of [Fe(HB(1,2,4-triazol-1-yl)$_3$)$_2$] that were vacuum-deposited in the 20-200 nm thickness range, showed an abrupt SCO without any fatigue over more than 10 million thermal switching cycles, which could be exploited in photonic, electronic, sensor, actuator and temperature damping devices.[21,25–29] The synthesis of [Fe(HB(1,2,3-triazol-1-yl)$_3$)$_2$] **1** (Chart 1), a structural isomer of its 1,2,4-triazolyl counterpart, was described by Jenkins *et al.*,[30] but there is no report on the SCO properties of this compound. In order to find out how the change of exodentate nitrogen atom position from 4 to 3 in the triazolyl ring impacts crystalline structure and SCO properties of the complex, as well as to analyze its solvato/polymorphism, we report herein the single crystal structure of **1** (both in solvated and desolvated forms) as well as its physical properties investigated by Mössbauer spectroscopy and variable-temperature magnetic susceptibility, Raman spectroscopy powder X-ray diffraction, calorimetry and thermogravimetry methods. Review on polymorphism in spin crossover complexes has been reported by Tao et al.[31] Such polymorphs are generally obtained serendipitously as mixture of crystals as illustrated by works of Ruben and collaborators.[32] On the other hand, numerous examples of solvatomorphs in SCO complexes have been also reported mainly in polymeric Fe(II) Hofmann type and in molecular Fe(II) and Fe(III) compounds.[33-47] These solvatomorphs result from a mixture of crystals obtained serendipitously, by a vapor-induced single-crystal-to-single-crystal transformation or growing crystals by liquid–liquid diffusion methods. In the present case, solvatomorphs were

[a] Taras Shevchenko National University of Kyiv, Department of Chemistry, 64 Volodymyrska St. 01601Kyiv, Ukraine. E-mail: illia.guralskyi@univ.kiev.ua
[b] LCC, CNRS and Université de Toulouse (UPS, INP) 205 route de Narbonne, F-31077 Toulouse, France.
[c] "Petru Poni" Institute of Macromolecular Chemistry, 41A Aleea Gr. Ghica Voda, 700487 Iasi, Romania.
[d] Department of Material Science and New Technology, Vasyl Stefanyk Precarpathian National University, Ivano-Frankivsk 76018, Ukraine

† Electronic Supplementary Information (ESI) available: Table S1 crystal structure and refinement data for the solvatomorphs, Fig. S1-S4 crystal structures of some solvatomorphs with intermolecular interactions displayed, Fig. S5 packing diagram of **1·7DMSO**, Fig. S6 X-Ray diffraction patterns for DMSO solvatomorph, Fig. S7 TGA and DTA curves for **1·12H$_2$O**, Fig. S8 Simulated and experimental PXRD patterns of **1**, Fig. S9 Variable temperature Raman spectroscopy data for **1**, Fig. S10 Mössbauer spectra of **1·12H$_2$O** and polymorphs of **1**. CCDC 2161993-2161998. For ESI and crystallographic data in CIF or other electronic format see DOI: 10.1039/x0xx00000x

obtained by changing the solvent during the recrystallization procedure.

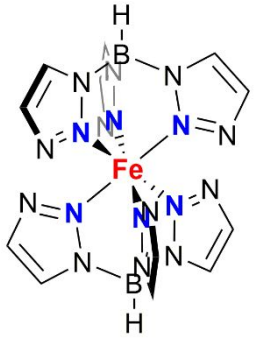

Chart 1 Molecular structure of $[Fe(HB(1,2,3\text{-triazlol-1-yl})_3)_2]$ (**1**).

Methods

Infrared spectrum was recorded on a Perkin Elmer 1725 spectrometer. Elemental analysis (for C, H and N) was performed using a Perkin Elmer 2400 series II Instrument. Single-crystal X-ray diffraction analysis was performed on an Oxford-Diffraction XCALIBUR E CCD diffractometer with graphite-monochromated Mo-Kα radiation. The unit cell determination and data integration were carried out using the CrysAlisPro package from Oxford Diffraction. Multi-scan correction for absorption was applied. All the structures were solved using an intrinsic phasing method using SHELXT and refined by full-matrix least-squares on F^2 with SHELXL[48,49] using the graphical interface of Olex2.[50] Non-hydrogen atoms were refined anisotropically. Aromatic hydrogen atoms were geometrically fixed and refined using a riding model. Variable temperature powder X-ray diffraction patterns were recorded using a Panalytical X'Pert diffractometer equipped with a Cu X-ray tube, a Ge(111) incident beam monochromator (λ = 1.5406 Å) and an X'Celerator detector. Variable-temperature Raman spectra were acquired by means of an Xplora (Horiba) Raman microspectrometer, using the 532 nm line of a Nd-YAG laser (0.1 mW). The sample temperature was controlled using a Linkam THMS600 liquid nitrogen cryostat. Differential thermal analysis and thermogravimetric (DTA–TG) data were acquired simultaneously using a Perkin-Elmer Diamond thermal analyzer under a 100 ml min^{-1} nitrogen flow at 10 K min^{-1}. DSC analysis was carried out on a Netsch DSC 3500 Sirius instrument under nitrogen purging gas (20 ml min^{-1}) at a heating/cooling rate of 10 K min^{-1}. Variable-temperature magnetic susceptibility data were obtained at cooling and heating rates of 2 K min^{-1} under a field of 1 kOe using a Quantum Design MPMS magnetometer. ^{57}Fe-Mössbauer spectra were recorded using a constant acceleration Mössbauer spectrometer with a ^{57}Co source. Fitting of the experimental data was performed with Recoil software.[51]

Materials and synthesis

Commercial reactants and solvents were used directly without further purification. The tris(1,2,3-triazolyl)borate ligand (NaL) and its neutral $[Fe(HB(1,2,3\text{-tz})_3)_2]$ iron (II) complex (hereafter FeL_2 or **1**) were synthesized according to experimental procedures reported in the literature[30]. The coordination compound isolated from the mother aqueous solution appears as dodecahydrate. The anhydrous powder form can be obtained *via* heating the hydrate above 90°C.

$FeL_2 \cdot 12H_2O$ (1·12H_2O). $C_{12}H_{38}B_2FeN_{18}O_{12}$ (M = 704.07). Anal. calc.: C, 20.47; H, 5.44; N, 35.81%. Found: C, 20.55; H, 5.42; N, 35.55%.

FeL_2 (1). $C_{12}H_{14}B_2N_{18}Fe$ (M = 487.88) Anal. calc.: C, 29.55; H, 2.89; N, 51.68%. Found: C, 29.51; H, 2.86; N, 51.57%.

Results and discussion

X-ray crystallography

Complex **1** is soluble in polar solvents, such as water, methanol, dimethylsulfoxide (DMSO), dimethylformamide (DMF) and poorly soluble in much less polar chloroform. The complex tends to form solvates, which can be easily crystallized from the above-mentioned solvents. The number of the solvent molecules per one molecule of the complex depends on the nature of the solvent. For instance, in the case of DMSO, the formation of two solvates **1·2DMSO** and **1·7DMSO** was observed serendipitously from attempts of recrystallization of **1** in the same condition. The methanol- or chloroform-based solvates appear only as **1·2MeOH** and **1·2$CHCl_3$**, respectively. The dimethylformamide solvate tends to crystallize with inclusion of one water molecule to form **1·2DMF·H_2O**. The solvatomorphs **1·2MeOH** and **1·2$CHCl_3$** crystallize in monoclinic space groups $P2_1/n$ and $P2_1/c$, respectively. **1·2DMF·H_2O** crystallizes in the orthorhombic *Pbcn* space group. In the case of DMSO-based solvatomorphs, **1·2DMSO** crystallizes in the triclinic $P\bar{1}$ space group, while **1·7DMSO** adopts a trigonal $R\bar{3}c$ space group. DMSO molecules in the latter crystals are disordered over six and over two positions, respectively. Upon long-term exposure to ambient air (~hours to days), crystals of solvatomorphs tend to lose their solvents. This process is followed by disintegration of the crystals along with structural changes and can be promoted by heating. Remarkably, crystals of **1·2$CHCl_3$** and **1·2MeOH** undergo single-crystal-to-single-crystal transformations upon heating. When heated at 313 K for one day, solvatomorph **1·2$CHCl_3$** completely loses its solvent to form stable crystals of **1**. The same transformation occurs in case of its methanol counterpart, but the latter requires heating at 323 K for two days. Incomplete solvent loss can be observed in **1·7DMSO**: after two days of evaporation, the single crystal degrades to powder, the diffraction pattern of which is consistent with the simulated one for **1·2DMSO** (Fig. S7).

The desolvated compound **1** crystallizes in the monoclinic $P2_1/c$ space group with 2 molecules of FeL_2 per unit cell (Fig. 1). It should be noted that the crystals used for refining the structure were obtained via a solid-state crystal-to-crystal transformation. This huge structural rearrangement is related to a chloroform solvent loss, namely c.a. 25% of the volumic contraction occurs (1412 to 1063 A^3) that leads to low quality multi-twin crystals. Three domains were considered upon the refinement. The room temperature (low spin state) unit cell

volume per molecule in the crystals of **1** (531.8 Å^3) is greater when compared to its 1,2,4-triazolyl isomer (516.6 Å^3).[52] While the structure of [Fe(HB(1,2,3-tz)$_3$)$_2$] is less dense, the mean intermolecular Fe···Fe separation (8.49 Å) is slightly shorter in **1** than in the 1,2,4-triazolyl isomer (8.87 Å). The coordination spheres of iron(II) ions in the solvatomorphs (as well as in **1**) have slightly distorted [FeN$_6$] octahedral geometries (see Table S2). The Fe–N distances lie in the range from 1.952(3) to

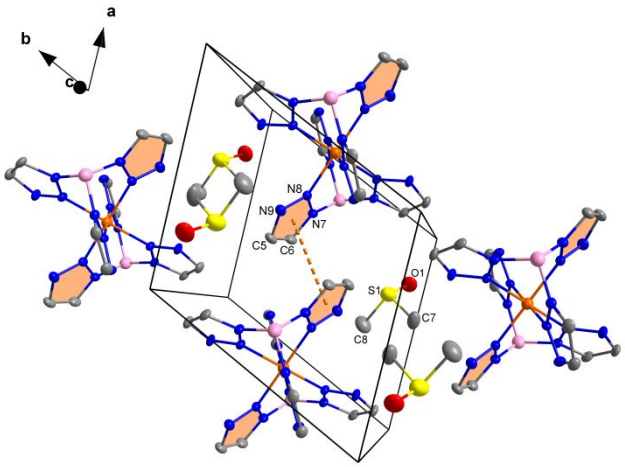

Fig. 1. Crystal structure of **1·2DMSO** showing intermolecular π-π stacking interactions developing along the *a* axis. Hydrogen atoms are omitted for clarity. Displacement elipsoids are drawn at 50% probability level.

1.972(2) Å, while the mean value of coordination octahedra volume (V$_p$) is 10.05 Å^3, as expected for the low spin iron(II).[53] Considering all the solvatomorphs, the average value of the octahedral distortion parameter $\sum|90^\circ - \theta_{N-Fe-N}|$ equals 21.66˚. Unfortunately, the high spin structure of **1** could not be assessed because crystals crash at the corresponding high temperatures. Indeed, single crystals of **1**, obtained *via* crystal-to-crystal transformation through thermally induced solvent loss, appear as low quality, highly cracked at room temperature, while further heating is a trigger for crystal degradation.

In the crystals of most of the solvatomorphs, as well as in **1**, π-π stacking interactions play a key role in the packing of FeL$_2$ molecules. The interactions occur between aromatic 1,2,3-triazolyl rings of adjacent complex molecules (Fig. 1, S1-S5). It is

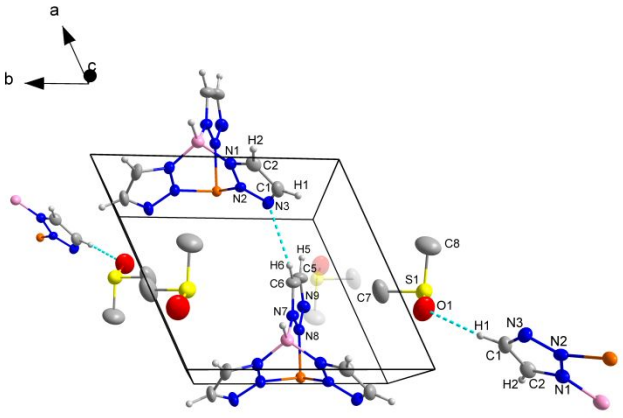

Fig. 2 Crystal structure of **1·2DMSO** showing intermolecular C–H···N and C–H···O contacts. Parts of the complex molecules are omitted for clarity. Displacement elipsoids are drawn at 50% probability level. Hydrogen atoms in the solvent molecules are omitted for clarity

noteworthy, that these interactions are spread along one direction in **1·2DMSO**, however they are bidirectional in **1** (Fig. S1) and in the rest of the solvatomorphs where they are observed. The centroid-centroid distances range from 3.560(3) to 3.6959(17) Å (Table 1). Another type of interactions that hold molecules of the complex together in the crystal lattices of **1** and **1·Solv** is represented by rather weak C–H···N interactions. The exodentate nitrogen atoms and C–H moieties of 1,2,3-triazolyl rings of neighboring FeL$_2$ molecules are involved in such intermolecular interactions (Fig. 2, S2-S5). Likely to π-π stacking interactions, C–H···N contacts propagate along a and b crystallographic directions (Fig. S2), however the structure of **1·2CHCl$_3$** reveals only a single propagation direction (Fig. S4). The parameters of the respective C–H···N contacts are gathered in Table 1. In **1·2DMSO** and **1·2DMF·H$_2$O**, the oxygen-containing polar solvents are bound to molecules of **1** *via* C–H···O contacts (Fig. 2, S5a). In **1·7DMSO**, the molecules of FeL$_2$ do not display any direct contacts with each other, but interact through solvent molecules by means of C–H···O contacts (Fig. S6). In **1·2MeOH**, a hydrogen bonding occurs involving the proton of the OH moiety of the solvent and the exodentate nitrogen atom of the triazolyl ring of the complex (d(O···N) = 2.867(4) Å, Fig. S3a). Chloroform molecules in **1·2CHCl$_3$** reveal C–H···N and C–H···Cl interactions with FeL$_2$ molecules (Fig. S4).

Table 1. Intermolecular FeL$_2$-FeL$_2$ interaction parameters.

π–π stacking interactions			
Compound	**C$_{ring}$–C'$_{ring}$ (Å)**	**C$_{ring}$–Plane' (Å)**	**Dihedral angle (°)**
1·2DMSO	3.640(4)	3.298(7)	25.03
1·2MeOH	3.560(3)	3.275(4)	23.08
1·2CHCl$_3$	3.6959(17)	3.375(3)	24.05
1·2DMF·H$_2$O	3.684(3)	3.377(4)	23.56
1	3.594(17)	3.28(3)	24.13
C–H···N interactions			
D–H···A	**D···A (Å)**	**∠(D–H···A) (°)**	
1·2DMSO			
C3–H3···N3	3.440(7)	150.0(3)	
C6–H6···N3	3.349(6)	137.6(3)	
1·2MeOH			
C2–H2···N6	3.279(4)	146.1(2)	
C6–H6···N3	3.196(4)	133.3(2)	
1·2CHCl$_3$			
C6–H6···N3	3.377(3)	153.97(14)	
1·2DMF·H$_2$O			
C2–H2···N6	3.290(4)	135.7(3)	
C4–H4···N9	3.345(4)	144.0(2)	
1			
C2–H2···N6	3.14(3)	150.4(17)	
C6–H6···N3	3.25(3)	134(2)	

Spin crossover properties

A plot of molar magnetic susceptibility as a function of temperature is shown on Figure 3. Temperature dependent magnetic measurements were conducted by first heating the powder of **1·12H$_2$O** from 250 K to 400 K, followed by cycling the as obtained dehydrated sample of **1** in the same temperature range at a rate of 2 K min^{-1}.

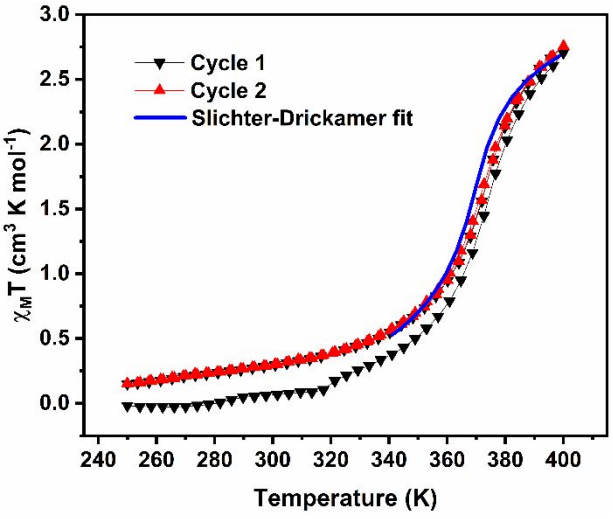

Fig. 3 $\chi_M T$ *vs* *T* plot, recorded over two thermal cycles starting with the powder sample **1·12H$_2$O**. Slichter-Drickamer fit was performed for the second heating curve.

Compound **1** undergoes a virtually complete, gradual spin crossover between the low spin (S = 0) and the high spin (S = 2) states, with a transition temperature $T_{1/2}$ = 373 K. We must note that the SCO is not fully completed at 400 K, which is the highest attainable temperature by our magnetometer, but variable-temperature Raman spectroscopic measurements conducted in the 303-433 K range reveal the flattening of the SCO curve slightly above 400 K (see Fig S9b). On the other hand, room temperature Mössbauer spectra recorded both for **1·12H$_2$O** and for the anhydrous powder **1** evidence only a low spin ferrous species (see Fig. S10). The variable temperature magnetic data could be conveniently fitted by the conventional Slichter-Drickamer (SD) model[37] (see Fig. 3), providing estimation of the enthalpy change (ΔH = 14 kJ mol^{-1}), entropy change (ΔS = 38 J K^{-1} mol^{-1}) and cooperativity (Γ = 5387 ± 52 J mol^{-1}) associated with the SCO phenomenon. One can remark here the relatively low entropy change and high cooperativity of the spin crossover in **1**, similar to the values reported previously for the 1,2,4-triazolyl isomer (ΔS = 48 J K^{-1} mol^{-1}, Γ = 5700 ± 50 J/mol).[54]

At first glance, one may ascribe the different magnetic behavior on the first heating to solvent loss. Indeed, TG-DTA data acquired for compound **1·12H$_2$O** reveals dehydration in the temperature range between ca. 313 and 363 K (Fig. 4). However, the DSC curve obtained for the hydrated powder displays several intense and broad endothermic peaks during the first heating (Fig. 5), which cannot be solely ascribed to the water loss, but denote also other (overlapped) physical phenomena, including obviously the SCO, but also various

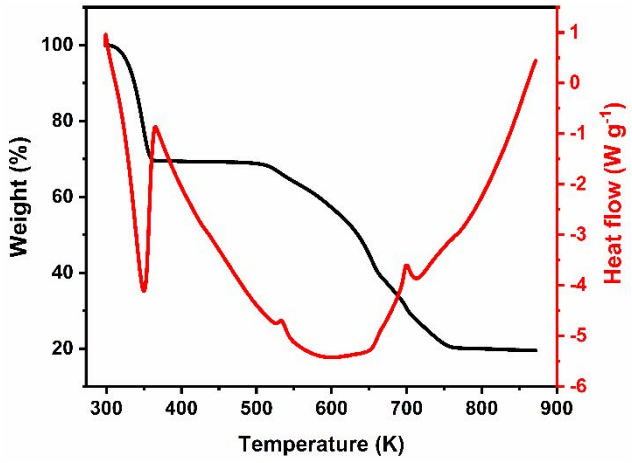

Fig. 4 TGA and DTA curves for **1·12H$_2$O**.

structural changes (vide infra). Remarkably, the DSC trace on cooling and on successive thermal cycling display a single exothermic (endothermic) peak at 366 K (373 K) on cooling (heating). The peak temperature as well as the associated enthalpy change of *ca* 14 kJ mol^{-1} agrees with the SD fit of the magnetic susceptibility data, allowing us to assign this peak to

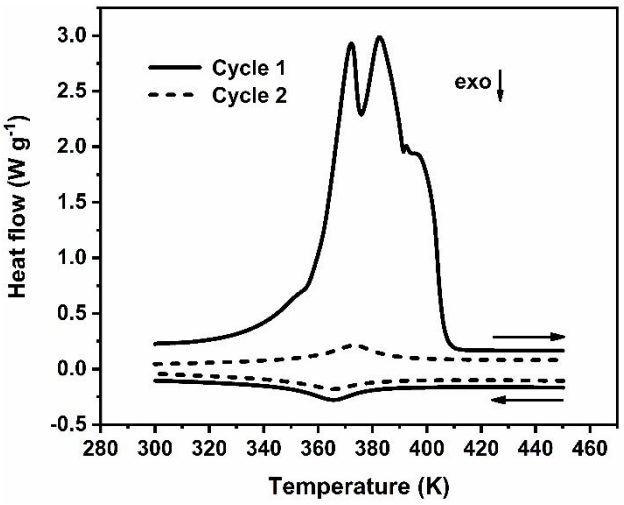

Fig. 5 DSC curves recorded starting with crystalline powder sample of **1·12H$_2$O** at 10 K min^{-1} rate over two successive heating/cooling cycles.

the sole SCO phenomenon.

In order to further investigate the possible interplay between solvent loss, structural changes and SCO in **1**, variable temperature powder XRD measurements were carried out in the 333-493 K temperature range following heating of **1·12H$_2$O** at 328 K for 1 h. The powder patterns recorded at 333, 363 and 393 K are substantially different – denoting successive dehydration/structural changes (Fig. 6). Of particular interest is that the experimental powder pattern recorded at 363 K shows the best match with the diffraction pattern simulated using the single crystal structural data of **1** (see Fig. S8). Then, further heating up to 493 K and cooling back to 303 K does not reveal any substantial change in the diffractograms (apart small shifts and broadenings of the peak positions – depending on the temperature). This finding is in line with the calorimetric and

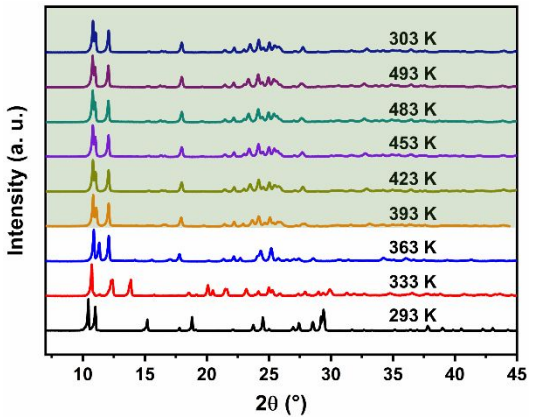

Fig. 6 Powder X-Ray diffraction patterns for bulk powders of **1·12H$_2$O** (293K) and **1** recorded at different temperatures.

magnetic measurements, pointing to the occurrence of a very gradual and reversible SCO following a first heating of the sample up to ca. 400 K.

Conclusions

In the present work, we report the crystal structures of solvated and desolvated forms of bis[hydrotris(1,2,3-triazol-1-yl)borate]iron(II) as well as their spin crossover properties. Similar to other unsubstituted tris(1-azolyl)borate iron(II) complexes, the complex exhibits reversible spin crossover above room temperature. The SCO in this complex is gradual and is centred at 373 K. Interestingly, the first heating of the hydrated complex is accompanied by a series of structural phase transitions resulting in different polymorphic phases of the compound. Crystal structures of the anhydrous complex and most of the solvatomorphs share the same types of interactions between the molecules of complex, including π-π stackings and weak C–H···N hydrogen bond interactions. In the course of this work, we have also evidenced the possibility of sublimating complex **1**, which opens attractive perspectives for the deposition of thin films and will be the matter of our further research.

Conflicts of interest

There are no conflicts to declare.

Acknowledgements

Authors acknowledge the financial support from the Ministry of Education and Science of Ukraine (grant 22BF037-09) and the courage of the Armed Forces of Ukraine that made the submission of this manuscript possible. We acknowledge Laure Vendier and Jean-Francois Meunier (LCC) for performing variable temperature PXRD and magnetic measurements, respectively. OYH acknowledges the French Embassy in Ukraine and Campus France for a BGF scholarship.

Notes and references

1 P. Gütlich, A. Hauser and H. Spiering, *Angew. Chemie Int. Ed. English*, 1994, **33**, 2024–2054.
2 P. Gütlich and H. A. Goodwin, Eds., *Spin Crossover in Transition Metal Compounds I*, Springer Berlin Heidelberg, Berlin, Heidelberg, 2004, vol. **233**-**235**.
3 M. A. Halcrow, Ed., *Spin-Crossover Materials: Properties and Applications*, John Wiley & Sons Ltd, Oxford, UK, 2013.
4 A. Bousseksou, Ed., Spin Crossover phenomenon, *Comptes Rendus Chim.*, 2018, **21**, 12, 1055–1300.
5 K. Senthil Kumar and M. Ruben, *Coord. Chem. Rev.*, 2017, **346**, 176–205.
6 G. Molnár, S. Rat, L. Salmon, W. Nicolazzi and A. Bousseksou, *Adv. Mater.*, 2018, **30**, 1–23.
7 K. S. Kumar and M. Ruben, *Angew. Chemie Int. Ed.*, 2021, **60**, 7502–7521.
8 L. Kipgen, M. Bernien, F. Tuczek and W. Kuch, *Adv. Mater.*, 2021, **33**, 2008141.
9 A. Pronschinske, R. C. Bruce, G. Lewis, Y. Chen, A. Calzolari, M. Buongiorno-Nardelli, D. A. Shultz, W. You and D. B. Dougherty, *Chem. Commun.*, 2013, **49**, 10446.
10 H. Naggert, J. Rudnik, L. Kipgen, M. Bernien, F. Nickel, L. M. Arruda, W. Kuch, C. Näther and F. Tuczek, *J. Mater. Chem. C*, 2015, **3**, 7870–7877.
11 V. Davesne, M. Gruber, M. Studniarek, W. H. Doh, S. Zafeiratos, L. Joly, F. Sirotti, M. G. Silly, A. B. Gaspar, J. A. Real, G. Schmerber, M. Bowen, W. Weber, S. Boukari, V. Da Costa, J. Arabski, W. Wulfhekel and E. Beaurepaire, *J. Chem. Phys.*, 2015, **142**, 194702.
12 M. Gruber, T. Miyamachi, V. Davesne, M. Bowen, S. Boukari, W. Wulfhekel, M. Alouani and E. Beaurepaire, *J. Chem. Phys.*, 2017, **146**, 092312.
13 M. Bernien, D. Wiedemann, C. F. Hermanns, A. Krüger, D. Rolf, W. Kroener, P. Müller, A. Grohmann and W. Kuch, *J. Phys. Chem. Lett.*, 2012, **3**, 3431–3434.
14 O. Iasco, M.-L. Boillot, A. Bellec, R. Guillot, E. Rivière, S. Mazerat, S. Nowak, D. Morineau, A. Brosseau, F. Miserque, V. Repain and T. Mallah, *J. Mater. Chem. C*, 2017, **5**, 11067–11075.
15 S. Rohlf, M. Gruber, B. M. Flöser, J. Grunwald, S. Jarausch, F. Diekmann, M. Kalläne, T. Jasper-Toennies, A. Buchholz, W. Plass, R. Berndt, F. Tuczek and K. Rossnagel, *J. Phys. Chem. Lett.*, 2018, **9**, 1491–1496.
16 T. Jasper-Tönnies, M. Gruber, S. Karan, H. Jacob, F. Tuczek and R. Berndt, *J. Phys. Chem. Lett.*, 2017, **8**, 1569–1573.
17 M. Atzori, L. Poggini, L. Squillantini, B. Cortigiani, M. Gonidec, P. Bencok, R. Sessoli and M. Mannini, *J. Mater. Chem. C*, 2018, **6**, 8885–8889.
18 T. Palamarciuc, J. C. Oberg, F. El Hallak, C. F. Hirjibehedin, M. Serri, S. Heutz, J.-F. Létard and P. Rosa, *J. Mater. Chem.*, 2012, **22**, 9690.
19 A. Mosey, A. S. Dale, G. Hao, A. N'Diaye, P. A. Dowben and R. Cheng, *J. Phys. Chem. Lett.*, 2020, **11**, 8231–8237.
20 S. Beniwal, S. Sarkar, F. Baier, B. Weber, P. A. Dowben and A. Enders, *J. Phys. Condens. Matter*, 2020, **32**, 324003.
21 V. Shalabaeva, S. Rat, M. D. Manrique-Juarez, A.-C. Bas, L. Vendier, L. Salmon, G. Molnár and A. Bousseksou, *J. Mater. Chem. C*, 2017, **5**, 4419–4425.

22 T. Mahfoud, G. Molnár, S. Cobo, L. Salmon, C. Thibault, C. Vieu, P. Demont and A. Bousseksou, *Appl. Phys. Lett.*, 2011, **99**, 9–11.

23 L. Salmon, G. Molnár, S. Cobo, P. Oulié, M. Etienne, T. Mahfoud, P. Demont, A. Eguchi, H. Watanabe, K. Tanaka and A. Bousseksou, *New J. Chem.*, 2009, **33**, 1283.

24 S. Trofimenko, *Scorpionates: The Coordination Chemistry of Polypyrazolylborate Ligands*, Imperial College Press, 1999.

25 M. D. Manrique-Juarez, F. Mathieu, V. Shalabaeva, J. Cacheux, S. Rat, L. Nicu, T. Leïchlé, L. Salmon, G. Molnár and A. Bousseksou, *Angew. Chemie - Int. Ed.*, 2017, **56**, 8074–8078.

26 V. Shalabaeva, K. Ridier, S. Rat, M. D. Manrique-Juarez, L. Salmon, I. Séguy, A. Rotaru, G. Molnár and A. Bousseksou, *Appl. Phys. Lett.*, 2018, **112**, 013301.

27 Y. Zhang, K. Ridier, V. Shalabaeva, I. Séguy, S. Pelloquin, H. Camon, S. Calvez, L. Routaboul, L. Salmon, G. Molnár and A. Bousseksou, *J. Mater. Chem. C*, 2020, **8**, 8007–8011.

28 K. Ridier, Y. Zhang, M. Piedrahita-Bello, C. M. Quintero, L. Salmon, G. Molnár, C. Bergaud and A. Bousseksou, *Adv. Mater.*, 2020, **32**, 1–5.

29 K. Ridier, A. C. Bas, Y. Zhang, L. Routaboul, L. Salmon, G. Molnár, C. Bergaud and A. Bousseksou, *Nat. Commun.*, 2020, **11**, 1–9.

30 B. C. Hughes, Z. Lu and D. M. Jenkins, *Chem. Commun.*, 2014, **50**, 5273–5275.

31 J. Tao, R.-J. Wei, R.-B. Huang and L.-S. Zheng, *Chem. Soc. Rev.*, 2012, **41**, 703–737.

32 I. Šalitroš, O. Fuhr, M. Ruben, *Materials*, 2016, **9**, 585.

33 M. Ohba, K. Yoneda, G. Agustí, M. C. Muñoz, A. B. Gaspar,J. A. Real, M. Yamasaki, H. Ando, Y. Nakao, S. Sakaki and S. Kitagawa, *Angew. Chem.*, 2009, **121**, 4861–4865.

34 J. J. M. Amoore, S. M. Neville, B. Moubaraki, S. S. Iremonger, K. S. Murray, J.-F. Létard and C. J. Kepert, *Chem. Eur. J.*, 2010, **16**, 1973–1982.

35 R.-J. Wei, B. Li, J. Tao, R.-B. Huang, L.-S. Zheng and Z. Zheng, *Inorg. Chem.*, 2011, **50**, 1170–1172.

36 C. Bartual-Murgui, A. Akou, H. J. Shepherd, G. Molnár, J. A. Real, L. Salmon and A. Bousseksou, *Chem. Eur. J.*, 2013, **19**, 15036–15043.

37 J. S. Costa, S. Rodríguez-Jiménez, G. A. Craig, B. Barth, C. M. Beavers, S. J. Teat and G. Aromí, *J. Am. Chem. Soc.*, 2014, **136**, 3869–3874.

38 R. Kulmaczewski, H. J. Shepherd, O. Cespedes and M. A. Halcrow, *Inorg. Chem.*, 2014, **53**, 9809–9817.

39 R. Kulmaczewski, J. Olguín, J. A. Kitchen, H. L. C. Feltham, G. N. L. Jameson, J. L. Tallon and S. Brooker, *J. Am. Chem. Soc.*, 2014, **136**, 878–881.

40 A. Santoro, L. J. Kershaw Cook, R. Kulmaczewski, S. A. Barrett, O. Cespedes and M. A. Halcrow, *Inorg. Chem.*, 2015, **54**, 682–693.

41 M. B. Bushuev, D. P. Pishchur, V. A. Logvinenko, Y. V. Gatilov, I. V. Korolkov, I. K. Shundrina, E. B. Nikolaenkova and V. P. Krivopalov, *Dalton Trans.*, 2016, **45**, 107–120.

42 S. Rodríguez-Jiménez, H. L. C. Feltham and S. Brooker, *Angew. Chem., Int. Ed.*, 2016, **55**, 15067–15071.

43 C. Bartual-Murgui, C. Codina, O. Roubeau and G. Aromí, *Chem. Eur. J.*, 2016, **22**, 12767–12776.

44 A. Djemel, O. Stefanczyk, M. Marchivie, E. Trzop, E. Collet, C. Desplanches, R. Delimi,G. Chastanet, *Chem. Eur. J.* 2018, **24**, 14760 – 14767.

45 T. Boonprab, P. Harding, K. S. Murray, W. Phonsri, S. G. Telfer, A. Alkaş, R. Ketkaew, Y. Tantirungrotechai, G. N. L. Jameson, D. J. Harding, *Dalton Trans.*, 2018, **47**, 12449.

46 S. Vela, H. Paulsen, *Dalton Trans.*, 2019, **48**, 1237-1245.

47 F.-L. Yang, W.-H. Wu, Y.-Q. Wang, X. Chen, B.-B. Liang, H.-L. Mi, G.-L. Zhang, X.-Y. Chen, Y. Shi, *Cryst. Growth Des*. 2021, **21**, 6671−6683

48 G. M. Sheldrick, *Acta Crystallogr. Sect. C Struct. Chem.*, 2015, **71**, 3–8.

49 G. M. Sheldrick, *Acta Crystallogr. Sect. A Found. Crystallogr.*, 2008, **64**, 112–122.

50 O. V. Dolomanov, L. J. Bourhis, R. J. Gildea, J. A. K. Howard and H. Puschmann, *J. Appl. Crystallogr.*, 2009, **42**, 339–341.

51 K. Lagarec and D. G. Rancourt, *Nucl. Instruments Methods Phys. Res. Sect. B Beam Interact. with Mater. Atoms*, 1997, **129**, 266–280.

52 S. Rat, K. Ridier, L. Vendier, G. Molnár, L. Salmon and A. Bousseksou, *CrystEngComm*, 2017, **19**, 3271–3280.

53 P. Guionneau, M. Marchivie, G. Bravic, J.-F. Létard and D. Chasseau, in *Spin Crossover in Transition Metal Compounds II*, eds. P. Gütlich and H. A. Goodwin, Springer Berlin Heidelberg, Berlin, Heidelberg, 2004, pp. 97–128.

54 C. P. Slichter and H. G. Drickamer, *J. Chem. Phys.*, 1972, **56**, 2142–2160.